Global phase diagram for a Van der Waals model of a binary mixture

D. Furman* and Robert B. Griffiths
Physics Department, Carnegie-Mellon University, Pittsburgh, Pennsylvania 15213
(Received 19 October 1977)

The Van der Waals model of a binary mixture in which b is constant and a depends quadratically on the composition possesses a global phase diagram in a space of five thermodynamic fields. The salient features of this phase diagram are worked out and compared with those found previously in a three-component model.

I. INTRODUCTION

The Van der Waals model[1] of a binary mixture has been studied extensively by Scott and Van Konynenberg.[2-4] In this paper we shall examine its global phase diagram in the particular case where the volume of close packing b is independent of composition and the Van der Waals parameter a is a quadratic function of composition. Under these conditions the Van der Waals model is very similar to a three-component model which we studied previously[5] if one of the three components is labeled "vacuum," and the principal purpose of this paper is to point out the similarities between the global phase diagrams of the two systems, as well as some significant differences.

The global phase diagrams are surprisingly similar and the main differences can be accounted for by the fact that the Van der Waals model has a lower symmetry than the three-component model and possesses a stronger singularity near close packing. While we give numerical values for some of the more outstanding singularities (such as tricritical points) in the global phase diagram of the Van der Waals model, our main emphasis, just as in the three-component model, is on the topological properties of the diagram and the different sorts of qualitative behavior possible in different regions of the parameter space.

Our results are in agreement with those of Scott and Van Konynenburg[2-4] when b is constant (they also considered situations where b depends on composition), with two exceptions. We find that the Van der Waals model possesses a "shield" region of four-phase coexistence which has not been pointed out previously. Also there are regions, so small as to be of little practical importance, near two of the lines of tricritical points where the binary system phase diagrams differ from those described by Scott and Van Konynenburg. These features have been studied independently by Scott,[6] who has reached conclusions identical to ours.

Our numerical methods were essentially identical with those we used for the three-component model, and the final results rather similar. Hence we shall omit details of the former and present a somewhat abbreviated account of the latter, stressing features in which the three-component and Van der Waals models are different.

An outline of the paper is as follows. The Van der Waals model is introduced in Sec. II together with certain variables and some notation used later in the paper. Section III is a discussion of the global phase diagram. Section III A describes our method of graphical representation of various features in the phase diagram, and Sec. III B describes the principal entities found in the five-dimensional space. Qualitative features of various system phase diagrams (associated with particular binary mixtures) are discussed in Sec. III C. Section III D contains qualitative information on various manifolds. Our principal conclusions are summarized in Sec. IV.

II. MODEL AND NOTATION

The Van der Waals model of a binary mixture of N_1 moles of component 1 and N_2 moles of component 2 is defined by the Helmholtz free energy

$$A = -NRT\ln(V-Nb) - aN^2/V + RTN(x_1\ln x_1 + x_2\ln x_2) + N[x_1 f_1(T) + x_2 f_2(T)], \tag{2.1}$$

where T, V, and R are the temperature, volume, and gas constant, respectively,

$$N = N_1 + N_2, \quad x_1 = N_1/N, \quad x_2 = N_2/N = 1 - x_1, \tag{2.2}$$

and f_1 and f_2 are functions which play no role in phase equilibria. By differentiating (2.1) with respect to V we obtain the well-known Van der Waals equation of state

$$p = \frac{-\partial A}{\partial V} = \frac{NRT}{V-Nb} - \frac{aN^2}{V^2}. \tag{2.3}$$

However, if the mixture a and b are assumed to depend on the mole fractions and x_2. We shall assume that b is a constant and a has a quadratic

dependence given by

$$a = a_{11}x_1^2 + 2a_{12}x_1x_2 + a_{22}x_2^2 . \tag{2.4}$$

To facilitate comparison with the three-component model, we rewrite (2.1) in the form

$$\begin{aligned}\bar{\alpha} &= Ab/RTV \\ &= r_1 \ln r_1 + r_2 \ln r_2 - (r_1 + r_2)\ln(1 - r_1 - r_2) \\ &\quad -(RT)^{-1}[a_{11}r_1^2 + 2a_{12}r_1r_2 + a_{22}r_2^2] + r_1\bar{f}_1(T) + r_2\bar{f}_2(T) ,\end{aligned} \tag{2.5}$$

where

$$r_1 = bN_1/V, \quad r_2 = bN_2/V \tag{2.6}$$

are dimensionless measures of density, and $\bar{\alpha}$ is a dimensionless free energy. In addition, let us define a free energy

$$P_\sigma = \bar{a}yz + \bar{b}xz + \bar{c}xy + x\ln x + y\ln y + (z - \sigma)\ln z \tag{2.7}$$

and make the identification

$$\begin{aligned}&x = r_1, \quad y = r_2, \quad z = 1 - r_1 - r_2 = 1 - x - y , \\ &\bar{a} = a_{22}/RT, \quad \bar{b} = a_{11}/RT, \quad \bar{c} = (a_{11} - 2a_{12} + a_{22})/RT.\end{aligned} \tag{2.8}$$

When $\sigma = 0$, P_0 is identical with the dimensionless Gibbs potential $\bar{G}$ which was our starting point for discussing the three component model—see Eq. (2.3) of Ref. 5. When $\sigma = 1$, P_1 is identical with $\bar{\alpha}$ in (2.5) if one makes a suitable choice of $\bar{f}_1(T)$ and $\bar{f}_2(T)$. (As these functions have no effect on phase coexistence, we shall hereafter ignore them.) Thus, the only difference between the three-component model and the Van der Waals model with b constant and a given by (2.4) is that the latter possesses an additional term, $-\ln z$, in the free energy (2.7).

While it is customary to employ "density" variables[7] such as x_1 and N/V in constructing phase diagrams of binary mixtures, for our purposes it is satisfactory and a considerable simplification to employ "field" variables which are always identical in coexisting phases. In particular, for drawing phase diagrams we shall employ the normalized "activity" variables (corresponding to ζ_x, ζ_y, and ζ_z of Ref. 1)

$$\zeta_1 = \bar{\zeta}^{-1}e^{\nu_1}, \quad \zeta_2 = \bar{\zeta}^{-1}e^{\nu_2}, \quad \zeta_0 = \bar{\zeta}^{-1}e^{-pb/RT} , \tag{2.9}$$

whose sum is equal to one if we let

$$\bar{\zeta} = e^{\nu_1} + e^{\nu_2} + e^{-pb/RT} . \tag{2.10}$$

Here ν_1 and ν_2 are the dimensionless chemical potentials of components 1 and 2 given by the formulas

$$\nu_1 = \frac{\mu_1}{RT} = \frac{\partial\bar{\alpha}}{\partial r_1} = \ln\left(\frac{x}{z}\right) + \frac{1}{z} + \bar{b}(z - x) + (\bar{c} - \bar{a})y , \tag{2.11}$$

$$\nu_2 = \frac{\mu_2}{RT} = \frac{\partial\bar{\alpha}}{\partial r_2} = \ln\left(\frac{y}{z}\right) + \frac{1}{z} + \bar{a}(z - y) + (\bar{c} - \bar{b})x .$$

Since $\bar{\alpha}$, and hence the location of coexisting phases, is obviously unaltered if T and the a_{ij} are simultaneously multiplied by the same factor, it is convenient, just as in Ref. 5, to *define* the temperature by

$$RT = (|\bar{a}| + |\bar{b}| + |\bar{c}|)^{-1} \tag{2.12}$$

and introduce normalized quantities

$$\hat{a} = RT\bar{a}, \quad \hat{b} = RT\bar{b}, \quad \hat{c} = RT\bar{c} \tag{2.13}$$

with

$$|\hat{a}| + |\hat{b}| + |\hat{c}| = 1 . \tag{2.14}$$

Note that these are related to Scott and Van Konynenburg's ζ and Λ parameters[2] through

$$\zeta = (\hat{a} - \hat{b})/(\hat{a} + \hat{b}), \quad \Lambda = \hat{c}/(\hat{a} + \hat{b}) \tag{2.15}$$

in the case where b is constant and $\hat{a}$ and $\hat{b}$ are non-negative (the only case we shall consider).

We shall use the symbol A^n to denote n coexisting phases, B a critical point, C a tricritical point, and D a fourth-order critical point. A critical end point (critical phase coexisting with a noncritical phase) is indicated by BA, etc.[8]

III. GLOBAL PHASE DIAGRAM

A. Sections, projections, and symmetries

The global phase diagram of the Van der Waals model may be thought of as a set of manifolds (curved lines, surfaces, etc.) of A^2, B, C, etc., in a five-dimensional space spanned by the field variables $\bar{a}$, $\bar{b}$, $\bar{c}$, ν_1, and ν_2. Graphical representation requires the use of projections of this diagram onto spaces of lower dimensionality, or sections of the full diagram holding one or more field variables fixed.

An example of a possible two-dimensional section with $\bar{a}$, $\bar{b}$, and $\bar{c}$ held fixed is shown in Fig. 1. One should think of this as a particular binary mixture at a fixed temperature with variable composition and density. Figure 1(a) uses a barycentric representation with weights x, y, and z given by (2.8). Thus the z vertex corresponds to vacuum, the x vertex to pure component 1 at close packing, the xz edge to pure component 1, etc. The regions of two-phase coexistence show that T is below the critical temperature of pure component 1 and above that of pure component 2, and the mixture separates into two fluid phases near

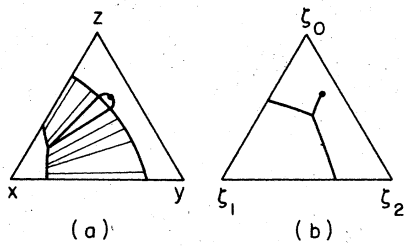

FIG. 1. (a) A phase diagram in the composition triangle. (b) The corresponding diagram in the activity triangle.

close packing. Three phase coexistence and a critical point occur at intermediate densities.

The same *qualitative* information is presented, somewhat more compactly, in the "activity" triangle of Fig. 1(b), with weights ζ_j defined in (2.9). The vertices ζ_0, ζ_1, and ζ_2 correspond to vacuum and close packing of components 1 and 2, respectively, the $\zeta_0\zeta_1$ edge corresponds to pure component 1, etc.

Figure 2(a) represents a *system* phase diagram, a three dimensional section of the global phase diagram at fixed $\hat{a}$, $\hat{b}$, and $\hat{c}$. It corresponds to a particular binary mixture in which T, p, and composition are all allowed to vary. [One can think of Fig. 1(b) as a section of Fig. 2(a) at a fixed value of T.] The two-phase coexistence surfaces Σ_1 and Σ_2 terminate in critical lines σ_1 and σ_2, respectively, and intersect along a triple line τ which joins σ_2 at a critical end point.

The system phase diagram can be projected on a p, T plane, Fig. 2(b), which is a common way of presenting information on phase equilibria in binary mixtures.[9] The lines labeled 1 and 2 are the liquid-vapor coexistence lines of the pure components and correspond to the edges of the Σ_1 and Σ_2 surfaces at $\zeta_2 = 0$ and $\zeta_1 = 0$, respectively, in Fig. 1(a). The critical line σ_1 originating at the critical point of pure component 1 goes to infinite pressure in Fig. 1(b) corresponding to close packing, $\zeta_0 = 0$, in Fig. 1(a). One can also project the system phase diagram in Fig. 1(a)

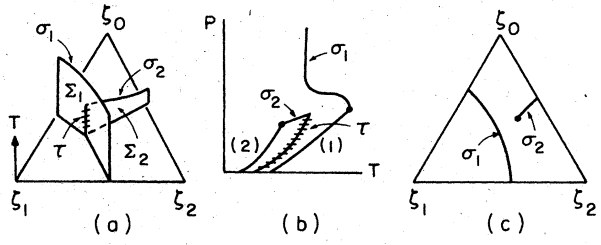

FIG. 2. (a) A system phase diagram in a triangular prism. (b) The diagram projected on the P-T plane. (c) The critical lines in (a) projected onto the base of the prism.

onto the base of the prism, as shown in Fig. 1(c) where only the critical lines are indicated.

Just as in Ref. 5, we shall use an "energy-space" projection of the global phase diagram along ν_1 and ν_2 onto the three-dimensional space spanned by $\bar{a}$, $\bar{b}$, and $\bar{c}$. In addition, we shall project the energy space along T onto two triangles. The triangle P corresponds to positive $\hat{a}$, $\hat{b}$, and $\hat{c}$, and these quantities are used as barycentric weights at the three vertices. The triangle Q, for $\hat{a} \geq 0$, $\hat{b} \geq 0$, and $\hat{c} \leq 0$, has barycentric weights $\hat{a}$, $\hat{b}$, and $-\hat{c}$. The triangles are shown, attached to each other along the $\hat{a}\hat{b}$ edge, in Fig. 3. One can also regard either triangle as the base of a prism with vertical axis equal to the temperature.

In our discussion of the three-component model we introduced six additional triangles in which $\hat{a}$ and $\hat{b}$ are allowed to be negative. As these would correspond to a negative Van der Waals a for a pure substance, which seems unphysical, we have omitted them in this paper. The use of triangles facilitates comparison with the three-component model, where they are useful in representing the symmetry, but for the Van der Waals model by itself the coordinates of Scott and Van Konynenburg, (2.15), are equally good and for some purposes preferable.

The normalized free energy (2.5), apart from the factors $\bar{f}_j(T)r_j$ (which are irrelevant for phase coexistence), is invariant under the simultaneous

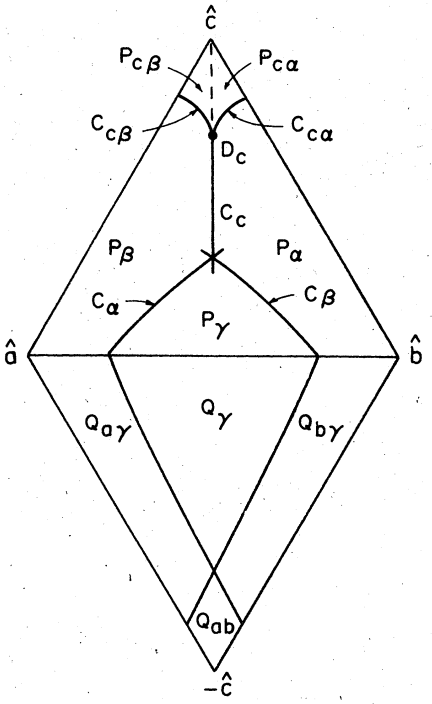

FIG. 3. Projection of the global phase diagram on the energy triangles.

interchange of r_1 with r_2 and a_{11} with a_{22}. In the notation of (2.7), this corresponds to interchanging x with y and $\bar{a}$ with $\bar{b}$. Thus, the global phase diagram is symmetric under the simultaneous interchange of $\bar{a}$ with $\bar{b}$ and ν_1 with ν_2, and the three-dimensional section $\bar{a}=\bar{b}$, $\nu_1=\nu_2$ is a symmetrical section. That the symmetry is lower than that of the three-component model is an immediate consequence of a nonzero σ in (2.7).

B. Principal features of the global phase diagrams

Figure 3 shows a projection of some of the principal features of the global phase diagram of the Van der Waals model on the two energy triangles of physical interest. The "shield" region near the center of the upper (P) triangle is shown on an expanded scale in Fig. 4. The corresponding diagrams for the three-component model are shown, for comparison, in Fig. 5.

The solid lines in Figs. 3 and 4 which are not edges of triangles are projections of lines of tricritical points C. Three of these lines meet at the fourth-order critical point D_c, but elsewhere the C lines do not intersect each other in the global diagram, though they appear to do so in the projection. The C lines are smooth curves in the full five-dimensional space, and the bends in C_α and C_β in passing from the P to the Q triangle are consequences of the projection.

The dashed line in Fig. 3 is the projection of an A^4 region bounded by lines of B^2 and BA^2 in a manner qualitatively identical to that found in the three-component model (see Fig. 8 of Ref. 5). In Fig. 4 the dashed curves are lines of BA^2 which bound a two-dimensional surface of A^4 in a manner which is qualitatively the same as in the three-component model. Note, however, that the shield region in the Van der Waals model, Fig. 4, has a twofold symmetry, reflection about the C_c line, in contrast to the threefold symmetry of the three-component model, Fig. 5(b). Also note that the BA^2 curves do not (in the full five-dimensional space) intersect the C curves except at the tricritical end points CA.

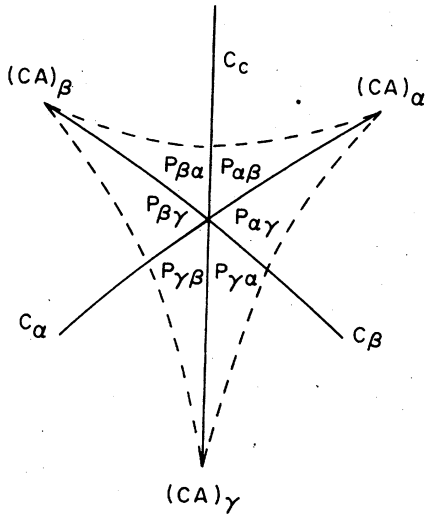

FIG. 4. Center of the upper (P) energy triangle enlarged.

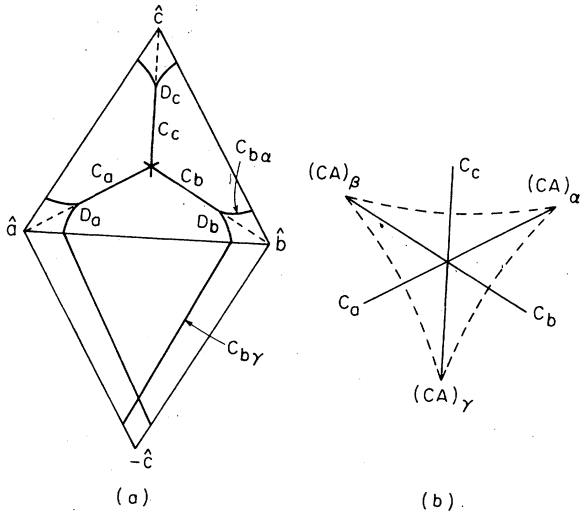

FIG. 5. (a) Projection of the global phase diagram of the three-component model on the energy triangles. (b) The center of the upper energy triangle enlarged.

The most important qualitative difference between the three-component and Van der Waals models is the absence in the latter of the point D_b in Fig. 5 and the joining of the two tricritical curves C_b and $C_{b\alpha}$ in Fig. 5 to form a single curve C_β in Fig. 3. (By symmetry, a similar change occurs at the left side of the diagram, where D_a disappears in the Van der Waals model.) Also, the A^4 region (dashed line) and $C_{b\alpha}$ curve in Fig. 5 are completely absent in the Van der Waals model.

To understand these differences it is helpful to imagine the continuous changes which take place in the global diagram as σ in (2.7) changes from 0 (Fig. 5) to 1 (Fig. 3). As soon as σ is nonzero the threefold symmetry of the three-component model disappears and with it the point D_b. The line $C_{b\alpha}$ and the A^4 region near the $\hat{b}$ vertex in Fig. 5 persist for very small positive values of σ, but rapidly disappear at zero temperature as σ increases, leaving a diagram which is qualitatively the same as Fig. 3. The sensitivity of the $C_{b\alpha}$ points to variation of σ arises from the fact that they occur at small values of z (i.e., near close packing), and the equations for a tricritical point involve fifth derivatives of (2.7), hence a term σ/z.[5]

By contrast, the shield region of Fig. 5(b) remains virtually unchanged, aside from a change in symmetry, as σ increases from 0 to 1. Indeed, we employed this fact to locate features of interest in the shield region of the Van der Waals model. Starting with the known location of $(CA)_\beta$ in the three-component model, $\sigma = 0$, σ was increased in small steps. For each new value of σ the location of $(CA)_\beta$ was determined by a numerical perturbation procedure starting with its position at the previous step.

The lines drawn in Figs. 3 and 4 divide the P and Q triangles into a set of two-dimensional regions which are labeled with subscripts (Q_γ, etc.) in a manner corresponding to that used for the three-component model.[5] The relationship to Scott and Van Konynenburg's notation, see in particular Fig. 1 of Ref. 2, is as follows. If we ignore the distinctions due to azeotropy (thus use I to denote both I and I-A), their regions I, II (apart from what we call the shield region), and V correspond to Q_γ, P_γ, and $Q_{\alpha\gamma}$, respectively, whereas regions III and IV together make up P_β. [Note that positive ζ, (2.15), and hence Fig. 1 of Ref. 2, corresponds to the *left* half of Fig. 3. We shall, however, use the notation I, II, etc. to denote the corresponding regions on either side of the symmetry axis.] One finds qualitatively different types of system phase diagrams in the different regions, as discussed below.

Quantitative values for various features are given in Table I.

C. Generic system phase diagrams

Associated with each point in the projection in Fig. 3 is a corresponding system phase diagram. Figure 6 shows a number of system phase diagrams associated with different points indicated (by square, etc.) in part (a) of the figure. All of these system diagrams, as well as those in Figs. 8 and 10, are *schematic*, drawn so as to indicate the topological structure rather than numerical magnitudes. All the diagrams in Fig. 6 are qualitatively the same as the corresponding diagrams in the three-component model. The greek letters labeling the critical end points in Figs. 6(b)–6(d) follow the same convention as Ref. 5. The labels in Figs. 6(e), 6(g), and 6(h) are different for reasons discussed below.

The system diagrams for points near the $\hat{c}$ vertex of the P triangle are qualitatively the same as in the three-component model. For this reason, and also because $\hat{c} > \frac{1}{2}$ corresponds to a negative, and hence, presumably, and unphysical value for a_{12} in (2.4), we shall not discuss them.

On the other hand, the system diagrams for points in the P triangle near the C_β tricritical

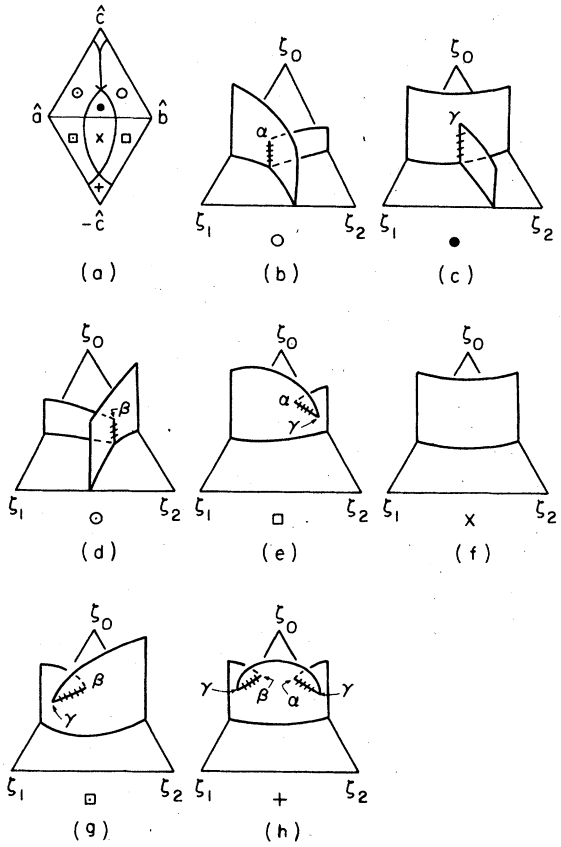

FIG. 6. System phase diagrams corresponding to the energy points shown in (a) are drawn schematically in (b)–(h).

line (and, by symmetry, those near C_α) differ from the corresponding three-component diagrams in some important respects. These can best be understood in terms of the behavior of the critical-end-point (BA) manifolds near the C_β line. Figure 7 shows three cuts or sections through the energy-space projection of the global phase diagram, regarded as a prism with a vertical T axis above a triangular base, indicated by C_0, C_1, and C_2 in Fig. 7(a).

The section C_0 is shown in Fig. 7(b), with α and β the corresponding BA manifolds. Because the cusp at the tricritical point is vertical or parallel to the T axis, a consequence of the symmetry of the global diagram, a given system phase diagram occurring at a fixed value of $\hat{b}$ (as well as $\hat{a}$ and $\hat{c}$) contains at most *one* critical end point, either one of type α or type β.

However, in the section C_1 shown in Fig. 7(c), there is not (in contrast to the three-component model) a corresponding symmetry, and the cusp is not vertical, but tilts slightly to the right, in the direction of the arrow in Fig. 7(a). The tilt is relatively small, but persists all the way from

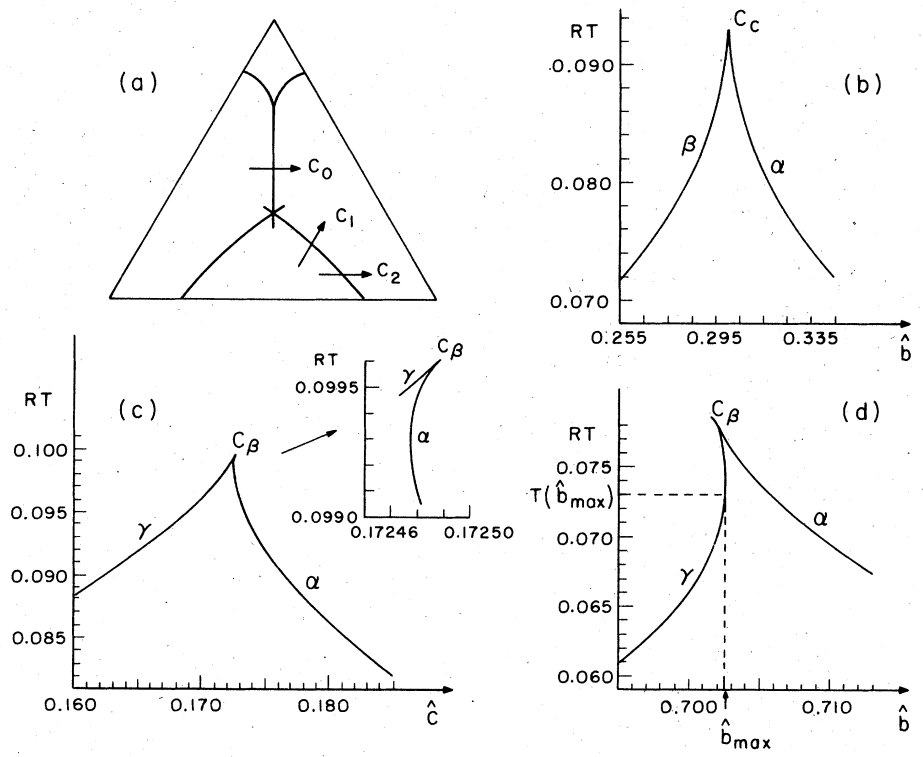

FIG. 7. For the three cuts labeled C_0, C_1, and C_2 in (a) the locations of the critical-end-point manifolds are shown in (b), (c), and (d), respectively. Cut C_0 is at $\hat{c} = 0.399\,57$, C_1 is at $\hat{b} = 0.568\,090\,931$, and C_2 is at $\hat{c} = 0.080\,040\,875$. Note that in (b), (c), and (d), increasing values of the abscissa correspond to the directions indicated by the arrowheads in (a).

the point $(CA)_\beta$ in Fig. 4 to the place where C_β intersects the geometrical mean curve

$$a_{12} = (a_{11}a_{22})^{1/2} \tag{3.1}$$

(the inscribed circle in Fig. 9), where the cusp is vertical.[6] Still closer to the $\hat{a}\hat{b}$ edge of the P triangle, the tilt is in the opposite direction, as shown by the section C_2 in Fig. 7(d).

The consequences of this tilting for system phase diagrams can be inferred from Fig. 7(d), which is similar to Fig. 3 of Ref. 2. For a fixed $\hat{c}$ corresponding to the section C_2 and for large values of $\hat{b}$, say the C_2 arrowhead in Fig. 7(a), there is only a single critical end point of α type, as in Fig. 6(b). This behavior persists as $\hat{b}$ decreases until it reaches the value $\hat{b}_{max}$ in Fig. 7(d), where two new γ-type BA points appear, as shown in Fig. 8(b). After a further small decrease of $\hat{b}$, one of

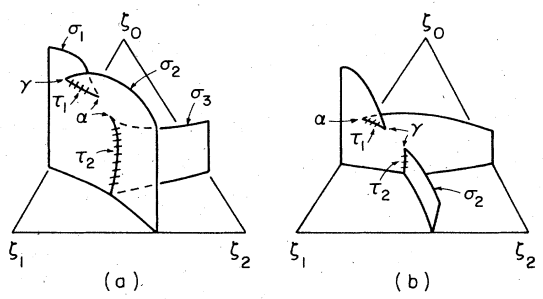

FIG. 8. Schematic system phase diagrams for systems having three critical end points, corresponding to appropriate portions of the cuts C_1 and C_2 in Fig. 7(a), are shown in (a) and (b), respectively.

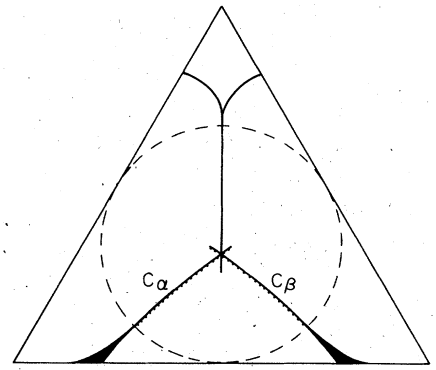

FIG. 9. Shaded region indicates, approximately, the extent of type-IV behavior as determined by Scott and Van Konynenburg. The additional, very narrow, regions where three critical end points arise are indicated schematically by the dots next to the C_α and C_β tricritical lines.

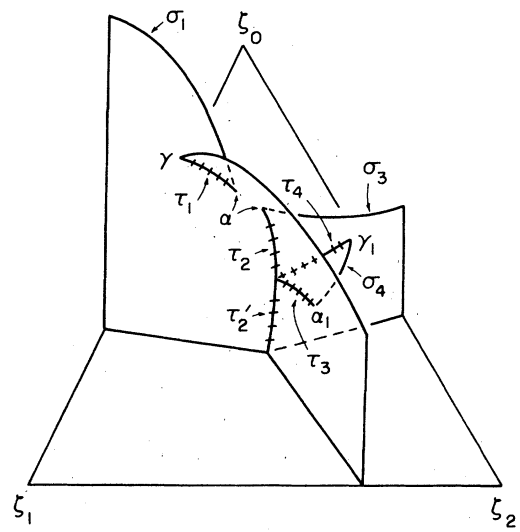

FIG. 10. Schematic system phase diagram in the shield region $P_{\gamma\alpha}$ very near C_β.

these joins the α-type BA and disappears at a tricritical point, leaving only a single γ-type BA, Fig. 6(c).

The region where three critical end points occur is labeled IV by Scott and Van Konynenburg.[2-4] Its extent is indicated, approximately, by the shaded region in Fig. 9. At the base of the triangle it does not extend all the way to the $\hat{b}$ vertex, but only up to[6]

$$\hat{b} = \tfrac{1}{2}(1 + 1/\sqrt{2}) \qquad (3.2)$$

(or $\zeta = -1/\sqrt{2}$ in the notation of Ref. 2).

By a completely analogous argument based on Fig. 7(c), one can see that just to the left of the C_β curve inside the inscribed circle in Fig. 9 there will be another small region, indicated schematically by dots, where system phase diagrams possess three critical end points: two of α type and one of γ, as in Fig. 8(a). The extent of this region is extremely small, as is evident from the scale on the inset in Fig. 7(c), and thus it is not surprising that it was overlooked by Scott and Van Konynenburg (though later found by Scott[6]).

The system phase diagrams for points in the shield region, Fig. 4, are identical with those in the three-component model apart from complications which arise due to the tilting of the BA cusps along the C_β and C_α curves. Figure 10, which contains five critical end points (and is, of course, schematic), shows one of these complications. It refers to a point very near the C_β line in the $P_{\alpha\gamma}$ region of Fig. 4.

D. Qualitative descriptions of various manifolds

Points of different types (C, BA, etc.) in the global phase diagram lie on various distinct smooth manifolds (curves, surfaces, etc.). We shall say that two manifolds related to each other by symmetry (as C_α and C_β, Fig. 3) belong to the same class. Table II lists one manifold from each class, with the exception of A^2 and B, and indicates the manifolds lying on its boundary. Here (e) indicates an intersection of the manifolds with a boundary of the phase diagram at finite temperature and (n) one at zero temperature.

The connectivity of different manifolds in the upper portion of the P triangle, including the shield region, is identical to that in the three-component model. Similarly, the connectivity in the Q triangle in both models is identical, apart from the $\hat{a}\hat{b}$ edge.

The qualitative differences between the models are as follows. The point D_b and the manifolds $C_{b\alpha}$ and $(A^4)_b$ associated with it in the $\hat{b}$ corner of the upper (P) triangle, Fig. 5(a), are completely absent in the Van der Waals model. Furthermore, the C_b and $C_{b\gamma}$ tricritical curves, which are distinct manifolds in the three-component model (Fig. 5) become a single manifold, labeled C_β in Fig. 3, in the Van der Waals model. Likewise the $(BA)_{b\gamma}$, $(BA)_{b\gamma}$, and $(A^3)_{b\gamma}$ manifolds, which terminate at the $C_{b\gamma}$ curve in the three-component model, in the Van der Waals model become continuous extensions of the $(BA)_\alpha$, $(BA)_\gamma$, and $(A^3)_{\rm I}$ manifolds, and have been labeled accordingly. By symmetry, the C_a and $C_{a\gamma}$ lines in the three-component model become a single C_α line in the Van der Waals model, and $(BA)_{a\gamma}$, $(BA)_{\gamma a}$, and $(A^3)_{a\gamma}$ become part of $(BA)_\beta$, $(BA)_\gamma$, and $(A^3)_{\rm I}$.

The energy-space projection of the $(BA)_\gamma$ manifold has some peculiarities which deserve comment. In the P_γ region it lies above (in T) the A^3 region at a given $\hat{a}$, $\hat{b}$, and $\hat{c}$. In the shaded regions in Fig. 9 (Scott and Van Konynenburg's IV) it doubles over so that it projects down twice on the P triangle; see Fig. 7(d). The lower branch, along with the entire manifold in the P_γ region, goes to zero temperature along the $\hat{a}\hat{b}$ edge of the P triangle. In the $Q_{b\gamma}$ region, on the other hand, the $(BA)_\gamma$ manifold lies below (in T) the A^3 region, and for $\hat{b}$ greater than the value in (3.2), it goes to zero temperature along the $\hat{a}\hat{b}$ edge of the Q triangle, whereas for slightly smaller $\hat{b}$ values it passes into the P triangle at a finite temperature to become the upper branch of the $(BA)_\gamma$ manifold in region IV. Analogous comments apply, by symmetry, to the $(BA)_\gamma$ manifold in the $Q_{a\gamma}$ region.

In the shield region the connectivity of the different manifolds in the Van der Waals model is precisely the same as in the three-component model. To supplement the description in Ref. 5, we include Fig. 11 which shows a section of the

TABLE I. Numerical values for selected entities. The first column gives the dimension d of the manifold indicated in the second column. The energy parameters $\bar{a}$, $\bar{b}$, $\bar{c}$ and the composition x and y of representative points are listed in the remaining columns. In the case of a compound entity x and y refer to the critical phase, and x' and y', and x'' and y'', to coexisting phases. (The notation 0.1873+1 means 0.1873×10^{1}, etc.)

		Location						
d	Manifold	$\bar{c}$	$\bar{b}$	$\bar{a}$	x	y	x'	y'
0	D_c	0.135 685 19+02	0.297 033 36+01	0.297 033 36+01	0.073 700	0.073 700		
1	$(CA)_\gamma$	0.333 330 81+01	0.479 174 84+01	0.479 174 84+01	0.300 002	0.300 002	0.054 087	0.054 087
1	$(CA)_\beta$	0.423 572 56+01	0.402 592 62+01	0.473 715 88+01	0.283 283	0.123 051	0.050 254	0.639 877
1	C_c	$\bar{c}$	$\frac{2\bar{c}-2\bar{c}^2-\bar{c}^3/2}{16\bar{c}-16-4\bar{c}^2}$	$\bar{b}$	$1/\bar{c}$	$1/\bar{c}$		
1	$C_{c\beta}$	0.154 266+02	0.287 105+01	0.311 639+01	0.170 023−01	0.161 970		
		0.161 284+02	0.215 048+01	0.317 547+01	0.961 841−02	0.186 451		
		0.161 718+02	0.138 619+01	0.320 003+01	0.728 297−02	0.196 912		
		0.160 136+02	0.685 302	0.321 460+01	0.607 164−02	0.203 295		
		0.157 771+02	−0.919 523−02	0.322 441+01	0.532 453−02	0.207 689		
		0.148 378+02	−0.191 377+01	0.324 326+01	0.404 145−02	0.216 401		
		0.135 163+02	−0.406 620+01	0.325 671+01	0.324 125−02	0.222 893		
		0.106 350+02	−0.814 667+01	0.327 267+01	0.241 176−02	0.230 985		
		0.643 796+01	−0.135 382+01	0.328 550+01	0.183 774−02	0.237 867		
		0.268 797+01	−0.181 062+02	0.329 292+01	0.154 267−02	0.242 037		
		−0.345 071+01	−0.253 179+02	0.330 130+01	0.124 099−02	0.246 958		
		−0.464 93 +03	−0.504 096+03	0.335 308+01	0.108 936−03	0.286 563		
1	C_β	0.390 544+01	0.409 468+01	0.442 088+01	0.278 841	0.133 951		
		0.372 110+01	0.413 975+01	0.424 579+01	0.275 999	0.140 920		
		0.355 095+01	0.418 667+01	0.408 532+01	0.273 097	0.148 024		
		0.319 052+01	0.430 785+01	0.375 013+01	0.265 854	0.165 728		
		0.263 409+01	0.458 682+01	0.325 311+01	0.250 416	0.203 236		
		0.228 732+01	0.486 367+01	0.296 697+01	0.236 544	0.236 544		
		0.175 768+01	0.564 658+01	0.261 770+01	0.202 865	0.314 647		
		0.120 301+01	0.789 609+01	0.264 412+01	0.126 209	0.456 786		
		0.794 801	0.994 664+01	0.293 132+01	0.529 829−01	0.504 732		
		0	0.109 440+02	0.307 459+01	0.232 771−01	0.490 788		
		−0.745 152	0.110 974+02	0.312 235+01	0.161 562−01	0.481 213		
		−0.157 125+01	0.109 924+02	0.315 286+01	0.123 404−01	0.473 819		
		−0.394 265+01	0.104 080+02	0.318 785+01	0.864 142−02	0.463 998		
		−0.541 767+01	0.921 878+01	0.321 498+01	0.625 354−02	0.455 262		
		−0.101 665+02	0.602 702+01	0.324 578+01	0.403 149−02	0.443 911		
		−0.127 731+02	0.407 939+01	0.325 616+01	0.339 691−02	0.407 939		
		−0.166 029+02	0.107 305+01	0.326 743+01	0.277 130−02	0.434 802		
		−0.226 960+02	−0.394 097+01	0.327 991+01	0.215 592−02	0.429 028		
		−0.576 261+02	−0.349 576+02	0.331 065+01	0.975 988−03	0.412 578		
		−0.383 395+04	−0.377 345+04	0.336 611+01	0.181 525−04	0.363 026		

TABLE I. (Continued)

			Location							
d	Manifold	$\bar{c}$	$\bar{b}$	$\bar{a}$	x	y	x'	y'	x''	y''
1	$(BA^2)_{\alpha\beta}$	4.106	4.402	4.402	0.1667	0.1667	0.5383	0.8301−01	0.8301−01	0.5383
		4.111	4.329	4.473	0.1784	0.1563	0.5108	0.9048−01	0.7586−01	0.5627
		4.124	4.260	4.539	0.1910	0.1475	0.4817	0.9770−01	0.6948−01	0.5833
		4.165	4.144	4.643	0.2177	0.1346	0.4214	0.1102	0.5955−01	0.6136
		4.187	4.100	4.680	0.2314	0.1300	0.3913	0.1150	0.5601−01	0.6239
		4.205	4.070	4.704	0.2435	0.1271	0.3654	0.1183	0.5364−01	0.6306
		4.218	4.050	4.720	0.2544	0.1252	0.3423	0.1206	0.5204−01	0.6305
1	$(BA^2)_{\alpha\gamma}$	4.130	4.130	4.688	0.3385	0.1336	0.1749	0.1118	0.5962−01	0.6183
		4.054	4.200	4.667	0.3515	0.1413	0.1484	0.1048	0.6712−01	0.6029
		3.976	4.268	4.653	0.3600	0.1495	0.1291	0.9821−01	0.7554−01	0.5867
		3.896	4.337	4.647	0.3657	0.1588	0.1133	0.9175−01	0.8549−01	0.5689
		3.812	4.408	4.647	0.3691	0.1692	0.1000	0.8538−01	0.9744−01	0.5488
		3.729	4.484	4.656	0.3700	0.1820	0.8801−01	0.7882−01	0.1128	0.5246
		3.629	4.560	4.673	0.3678	0.1966	0.7790−01	0.7256−01	0.1317	0.4970
		3.533	4.638	4.700	0.3615	0.2152	0.6885−01	0.6627−01	0.1573	0.4621
		3.429	4.720	4.740	0.3474	0.2418	0.6057−01	0.5983−01	0.1971	0.4122
		3.365	4.769	4.773	0.3294	0.2671	0.5611−01	0.5598−01	0.2389	0.3642

TABLE II. Manifolds and their boundaries. A representative example from each class of manifolds, with the exception of B and A^2, is listed in the first column, followed by its dimensionality d and the numbers of manifolds in the class. The last column gives the manifolds of dimension $d-1$ lying on its boundary. For $d=2$ the manifolds are listed in order proceeding continuously along the edge of the boundary. All manifolds at zero temperature are labeled (n) and manifolds which terminate on the edges of the energy triangle at finite temperature are labeled (e).

Manifold	d	s	Boundary
D_c	0	1	
$(CA)_\gamma$	0	1	
$(CA)_\beta$	0	2	
C_c	1	1	D_c, $(CA)_\gamma$
C_β	1	2	$(CA)_\beta$, (e)
$C_{c\beta}$	1	2	D_c, (e)
$(BA^2)_{\alpha\beta}$	1	1	$(CA)_\alpha$, $(CA)_\beta$
$(BA^2)_{\alpha\gamma}$	1	2	$(CA_\alpha$, $(CA)_\gamma$
$(B^2)_c$	1	1	D_c, (n)
$(BA^2)_c$	1	1	D_c, (n)
$(BA)_{c\beta}$	2	2	$(B^2)_c$, $C_{c\beta}$, (e)
$(BA)_{\beta c}$	2	2	$(BA^2)_c$, $C_{c\beta}$, (e)
$(BA)_\gamma$	2	1	$(BA^2)_{\alpha\gamma}$, $(BA^2)_{\beta\gamma}$, C_β, C_α, (n)
$(BA)_\beta$	2	2	$(B^2)_c$, C_c, $(BA^2)_{\gamma\beta}$, $(BA^2)_{\alpha\beta}$, C_α, (e)
$(A^4)_I$	2	1	$(BA^2)_{\alpha\beta}$, $(BA^2)_{\beta\gamma}$, $(BA^2)_{\alpha\gamma}$
$(A^4)_c$	2	1	$(B^2)_c$, $(BA^2)_c$
$(A^3)_{c\beta}$	3	2	$(BA)_{c\beta}$, $(BA)_{\beta c}$, $(A^4)_c$
$(A^3)_I$	3	1	$(BA)_\alpha$, $(BA)_\beta$, $(BA)_\gamma$, $(A^4)_c$, $(A^4)_I$, (n)

energy space as indicated in part (a) of the figure. Note that the BA manifolds, the solid lines in Fig. 11(b), only intersect at the BA^2 and C points in the full phase diagram. The other apparent intersections in the figure are a result of the projection.

IV. CONCLUSION

The principal qualitative differences between the three-component and Van der Waals models are associated with changes near the $\hat{a}$ and $\hat{b}$ vertices of the P triangle. The disappearance of the D points arises from a lower symmetry in the Van der Waals case. Perhaps more interesting is the vanishing of all the complicated structure associated with the A^4 regions near the $\hat{a}$ and $\hat{b}$ vertices of the three-component model. This is related, we feel, to the fact that Van der Waals model has a strong divergence of the pressure near close packing, in contrast to the relatively mild logarithmic divergence in the three component case. Presumably the Van der Waals behavior is the more realistic for real systems.

It is rather interesting that the shield region is

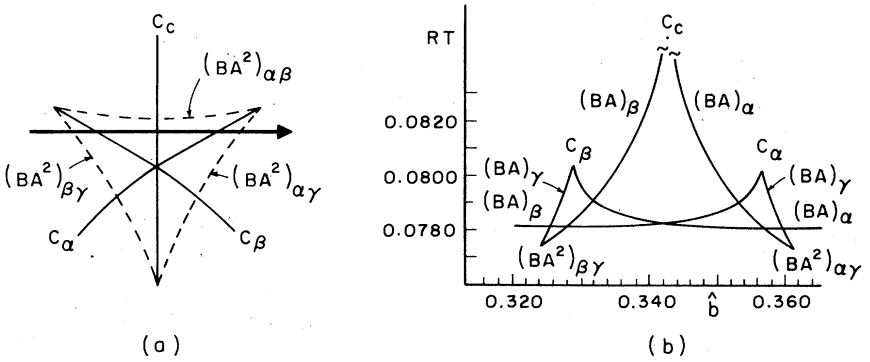

FIG. 11. Location of the critical-end-point manifolds in the temperature and $\hat{b}$ plane are shown in (b) for the cut indicated in (a) at $\hat{c} = 0.314\,866\,778\,8$, which crosses the shield region. Increasing values of the abscissa in (b) correspond to the direction indicated by the arrowhead in (a).

present in both models. Presumably it also persists in at least certain cases in which the Van der Waals b depends on composition. As we pointed out previously,[5] it is not altogether obvious that such a region can actually exist in real systems, and hence an experimental search for it might prove worthwhile.

In addition to basic changes in the topological structure of the global phase diagrams, certain differences between the Van der Waals and three-component models can be traced back to changes in symmetry, e.g., the appearance of the type-IV regions discussed in Sec. III C is related to the orientation of the BA cusp at a C point in relation to the temperature axis. It is our opinion that these differences are much less "fundamental", in that any reasonable application of the three-component model to real systems cannot presume that the latter will have the symmetry of the former.

ACKNOWLEDGMENTS

We have benefited from conversations with Professor J. C. Wheeler and Professor R. L. Scott. This research was supported by NSF Grant No. 76-23071.

---

*Present address: Bell Laboratories, Murray Hill, N. J. 07974.

[1]J. D. van der Waals, *Die Kontinuität des Gas Förmigen und Flüssigen Zustandes* (Barth, Leipzig, 1899).
[2]R. L. Scott and P. H. van Konynenburg, Discuss. Faraday Soc. 49, 87 (1970).
[3]R. L. Scott, Ber Bunsenges. Phys. Chem. 76, 296 (1972).
[4]P. H. Van Konynenburg, Critical Lines and Phase Equilibria in Binary Mixtures, Ph.D. dissertation, (UCLA, 1968) (unpublished).
[5]D. Furman, S. Dattagupta, and R. B. Griffiths, Phys. Rev. B 15, 441 (1977).
[6]R. L. Scott (private communication).
[7]The notation is that of R. B. Griffiths and J. C. Wheeler, Phys. Rev. A 2, 1047 (1970).
[8]R. B. Griffiths, Phys. Rev. B 12, 345 (1975).
[9]See, for example, J. S. Rowlinson, *Liquids and Liquid Mixtures* (Butterworths, London, 1959), Sec. 6.4.